Materials Science and Engineering A, (2016). http://dx.doi.org/10.1016/j.msea.2016.01.074

Experimental investigation of tension and compression creep-ageing behaviour of AA2050 with different initial tempers

Y. Li[1], Z. Shi[1,*], J. Lin[1], Y.-L. Yang[1], B.-M. Huang[2], T.-F. Chung[2] and J.-R. Yang[2]

[1]Department of Mechanical Engineering, Imperial College London, London SW7 2AZ, UK

[2]Department of Material Science and Engineering, National Taiwan University, Taiwan, ROC

Abstract: Creep-ageing behaviour of aluminium alloy 2050 with different initial tempers (T34, T84 and as-quenched) has been experimentally investigated under both tension and compression creep-ageing conditions, with different stress levels at 155 °C for 18 h. Corresponding strengthening phenomena have been studied by interrupted creep-ageing tests and subsequent tensile tests. Moreover, the microstructures of some selected specimens after creep-ageing tests have been examined by transmission electron microscopy (TEM) and the precipitation process has been analysed. It has been found that creep strains under tensile stresses are much larger than those under compressive stresses during the tests. A new "double primary creep feature" has been observed in both the as-quenched alloys and the pre-stretched/natural-aged (T34) alloys, in which an intermediate inverse creep stage with an increasing creep strain rate locates between the initial primary + transient steady-state creep stages and the second primary + second steady-state creep stages. While for the alloy with peak-aged initial temper (T84), typical primary and steady-state secondary creep stages are observed during tension creep-ageing tests and little creep strain occurs under compressive stresses of 150 and 175 MPa. The mechanisms for these phenomena are discussed in terms of microstructural interactions among the changing dislocations, solute-matrix bonding and precipitates, and their effects on the creep resistance of the alloy during creep-ageing tests are analysed.

Keywords: Creep-ageing; creep age forming; tension; compression; aluminium alloy 2050; initial temper

*Corresponding Author: Dr Zhusheng Shi

Email address: Zhusheng.Shi@Imperial.ac.uk Phone number: +44 (0)2075949546

Postal address: Department of Mechanical Engineering, Imperial College London, London SW7 2AZ, UK

1. Introduction

Creep age forming (CAF) is a process to deform aluminium alloys by keeping an external stress onto the material at an artificial ageing temperature for a specific time, thus simultaneously achieving high mechanical properties by age hardening and plastically forming the part within its elastic limit by creep deformation [1, 2]. It is an efficient way to manufacture extra-large light weight and high performance panel products in aerospace industry. Aluminium alloy 2050 (AA2050) is a third generation aluminium-copper-lithium (Al-Cu-Li) alloy which can achieve excellent strength-ductility performances by artificial ageing, leading to a great potential in aerospace applications [3, 4]. In order to manufacture AA2050 components with ideal mechanical properties through a CAF process, it is important to investigate the creep-ageing behaviour of the alloy. In a CAF process, a thick aluminium plate workpiece is mainly subjected to bending, in which one side of the material is in tension and the other side is in compression [1]. The study of the tension and compression creep-ageing behaviour of the alloy therefore becomes more important for CAF applications.

Although AA2050 is a recently-developed material [4] and has not been studied as thoroughly as some other aluminium alloys, its ageing behaviour can be referenced by the widely published studies of other Al-Cu-Li alloys with similar compositions [5, 6]. Generally, its main strengthening contribution comes from precipitation hardening [7]. The precipitates during the artificial ageing process can be summarised as GP zones, θ' (Al_2Cu), δ' (Al_3Li), S' (Al_2CuMg) and T_1 (Al_2CuLi), among which T_1 is mostly regarded as a main strengthening phase [8, 9]. Kumar et al. [8] have investigated the ageing process of Al-Cu-Li alloys with initial tempers of T3 and T4 and concluded that both precipitates from natural ageing and dislocations from pre-stretch in the initial temper would influence the subsequent ageing process. In addition, it has been reported that dislocations induced by the pre-stretch facilitate the nucleation of T_1 precipitates, thus accelerating ageing progress and promoting strength [10, 11]. By contrast, little research has been published on the creep behaviour of Al-Cu-Li alloys. Kazanjian et al. [12] have compared the creep curve of a Al-3.5Cu-1.0Li alloy with some other Al-Cu-Mg alloys and showed that all these alloys exhibit the typical two-stage (primary stage and steady secondary stage) creep behaviour and the Al-Cu-Li alloy presents a higher creep resistance than others. Nevertheless, the study has only considered the alloy with T8 initial temper and the creep behaviour of the alloy with other initial tempers has not been studied. As other initial tempers can be more important for the CAF process, such as the T34 initial temper of AA2050 which is solution heat-treated, pre-stretched and then naturally-aged,

the effects of different initial tempers on the creep-ageing behaviour which concerns both ageing and creep processes, therefore, necessitate further investigations.

In addition, both tensile and compressive stresses will appear in the material during the CAF process, but most of the studies now consider only the creep-ageing behaviour in tensile stress conditions [13, 14]. The stress directions have been demonstrated to affect the orientation of precipitates during the ageing process of some aluminium alloys [15, 16]. Eto et al. [15] and Zhu et al. [17, 18] have found that the main precipitates in Al-Cu alloys will adjust to be parallel with the direction of a tensile stress, while with a compressive stress, the preferential orientation tends to be perpendicular. However, creep tests of the material during these conditions were not included in their studies. Heimerl et al. [19] have reported a much larger creep strain in tension than in compression of the 2024-T3 (Al-Cu-Mg) alloy at elevated temperatures from 150 °C to 200 °C. The probable reasons have been proposed as both the pre-stretch and ageing effects. Moreover, Zhang et al. [20] and Przydatek [21] have observed the asymmetric tensile and compressive creep behaviour in Al-Si-Cu and Al-Cu-Mg alloys respectively and they both attributed the reason to the easier cavity nucleation on grain boundaries in tension creep conditions. As the precipitates in Al-Cu-Li alloys, such as θ' and T_1, have negative precipitate-matrix misfits which are believed to be the reason for the stress-orientation phenomena [15, 16], the tension and compression creep-ageing behaviour of such alloy may also be different. These phenomena require further investigations, so as to achieve the potential CAF applications of AA2050.

This study, for the first time, investigates and compares the creep-ageing behaviour of AA2050 with different initial tempers under both tensile and compressive stresses for their CAF applications. To investigate the interactions between the ageing and creep processes during creep-ageing tests, three initial tempers with different pre-stretch and initial ageing (natural-aged and peak-aged) conditions were studied. The results were analysed in detail by combining together the creep-ageing behaviour and the corresponding microstructural evolution observed in the experiments.

2. Experimental programme

2.1 Material and heat treatment conditions

The material used in the study is AA2050, whose chemical composition is listed in Table 1. The as-received material was in a T34 temper which had undergone solution heat-treatment (SHT) at 500 ^{o}C for 1 h, water-quenching (WQ), followed by 3.5-4.5% pre-stretching and natural ageing.

Table 1 Main chemical compositions of AA 2050 (wt.%).

Al	Cu	Li	Mg	Ag	Mn	Zr
Balance	3.6	0.9	0.34	0.35	0.34	0.08

In addition, other initial tempers were prepared in this study, which were achieved by re-heat treating the as-received material to particular tempers before creep-ageing tests. Fig. 1 shows schematically the heat treatment routes for different initial temper conditions. The initial tempers used in the study include:

T34: as-received (500 °C/1 h SHT + WQ + 3.5-4.5% pre-stretching + natural ageing);

T84: peak-aged (as-received + 155 °C/18 h artificial ageing to peak strength);

WQ: as-quenched (as-received + 500 °C/1 h SHT + WQ).

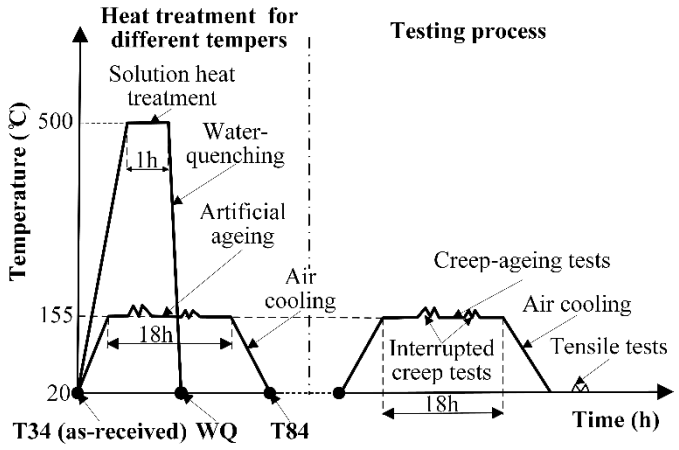

Figure 1. Schematic showing the heat treatment and test conditions.

Heat treatments were carried out using a Lenton AWF-13/5 chamber furnace to heat samples and keep them in the required temperature for a designated dwell time shown in Fig. 1. The T84 samples were air cooled after artificial ageing, while the WQ samples were water-quenched by immediately transferring them from the furnace to a cold water tank within 5 s.

2.2 Creep-ageing and mechanical testing

Same specimen design was used for both tension and compression creep-ageing tests, whose geometry is shown in Fig. 2. The specimens were machined from the centre of a 12.7 mm thick as-received plate along its rolling direction.

Both tension and compression creep-ageing tests were executed under a constant stress on an Instron 5584 machine with an assisting furnace. Two linear capacitance gauges were fitted onto the ridges of the specimen to measure the displacement during the tests. The 18-hour

creep-ageing tests of AA2050 with initial tempers of T34, WQ and T84 were carried out at stress levels of 150 and 175 MPa. Interrupted creep-ageing tests, including 2, 5, 8 and 12 h, and tests with extra-long creep-ageing time of 22 and 24 h were also carried out. All creep-ageing tests were conducted at a temperature of 155 °C and the temperature was controlled within ±3 °C. During the tests, the load was applied after the temperature of the specimen reached a steady state of 155 °C.

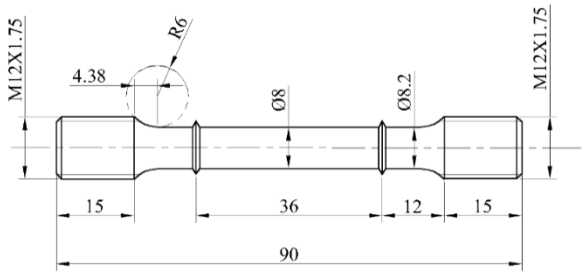

Figure 2. Specimen geometry for both tension and compression creep-ageing tests (Units: mm).

Room temperature tensile tests were conducted on the Instron 5584 machine at a strain rate of 10^{-4} s^{-1}. Hardness tests of the samples after pure ageing (without load) were carried out on a Zwick Roell hardness machine with an applied force of 10 kgf (HV10) holding for 10 s.

2.3 Transmission electron microscopy (TEM) observation

TEM observations were carried out for some selected specimens with T34 initial temper condition: the as-received material, 5 and 18 h tension creep-aged specimens under 150 MPa and 18 h compression creep-aged specimen under 150 MPa. The TEM specimens were prepared by cutting 3 mm diameter discs from the selected samples along the stress direction, thinning the discs mechanically to 0.08 mm afterwards and then twin-jet-electropolishing them to perforation with a mixture of 1/3 nitric acid and 2/3 methanol at -20 °C, using a potential of 10 V. The prepared TEM specimens were examined on a Tecnai F20 (200 kV) field-emission-gun transmission electron microscope (FEG-TEM). The stress direction in TEM specimens was marked to be a trace line by a knife. An example for the trace line of the stress direction is illustrated in Supplementary Figure 1 (Supplementary Material).

3. Experimental Results

3.1 Creep behaviour with different initial tempers

Fig. 3 shows the tension and compression creep-ageing curves of AA2050 for different initial tempers under applied stresses of 150 and 175 MPa for 18 h. Corresponding creep

strain rate curves for different initial tempers are presented in Fig. 4. The compression creep strain rate for T84 after 3 h is lower than 10^{-7} h^{-1} and is not plotted in Fig. 4(a). The alloy with the peak-aged initial temper (T84) exhibits the typical two-stage creep behaviour (Fig. 3(c)), which comprises of a primary creep stage where creep strain rate decreases quickly and a steady-state secondary creep stage with a relatively stable creep strain rate. Materials with non-peak-aged initial tempers, T34 (Fig. 3(a)) and WQ (Fig. 3(b)), show different behaviour from the typical two-stage creep curves: a particular stage with an increasing creep strain rate is observed during creep-ageing tests (Fig. 4). According to the trend of creep strain rate during the course of creep-ageing test (i.e., increasing, decreasing or relatively stable creep strain rates in Figs. 3 and 4), the creep-ageing curve of T34 specimens demonstrates a special five-stage (I, II, III, IV and V) phenomenon, whereas for WQ specimens, the stage V with a relatively stable creep strain rate is not observed (Fig. 4(b)). On the other hand, for the T84 initial temper condition, the conventional two-stage creep behaviour is clearly displayed in the corresponding trend of creep strain rate (Figs. 3(c) and 4(a)): including a primary creep stage (stage I') which is ended at about 3 h and a steady secondary creep stage (stage II') which lasts to the end of the test.

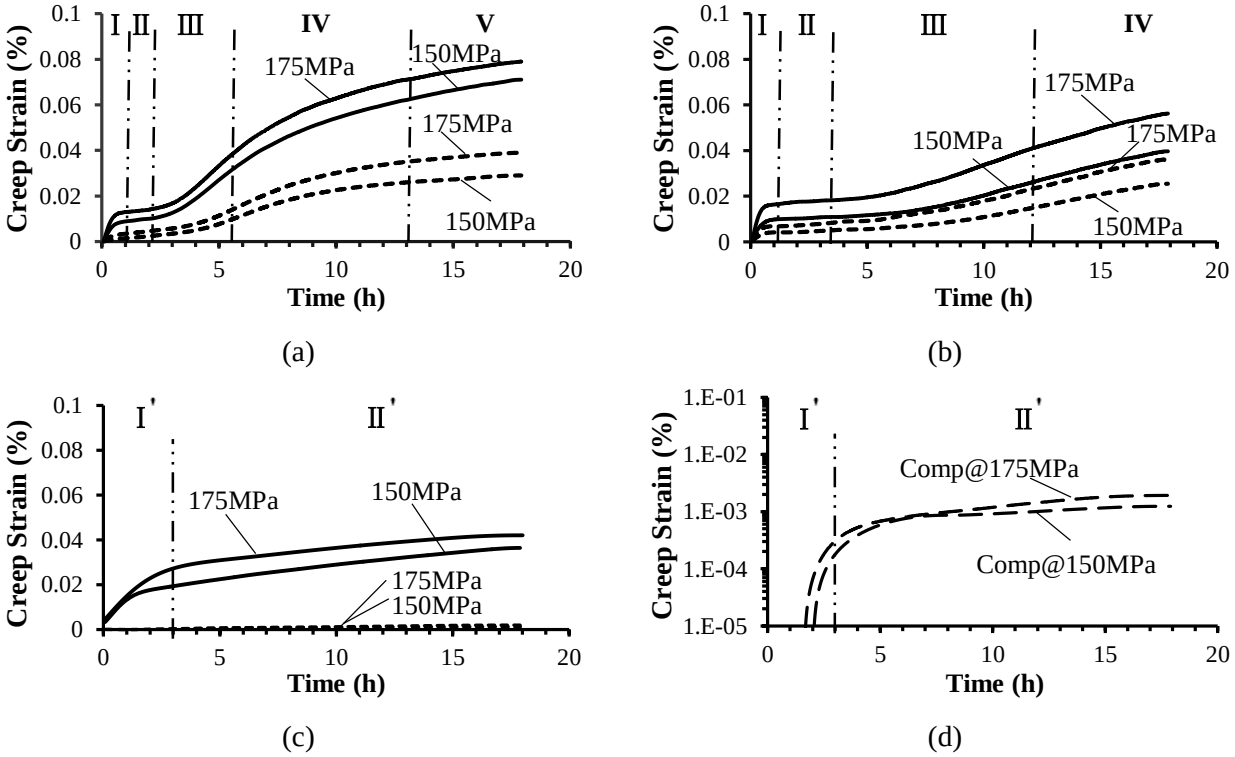

Figure 3. Tension (solid lines) and compression (dash lines) creep-ageing curves for (a) T34, (b) WQ and (c) T84 initial tempers under 150 and 175 MPa for 18 h. T84 compression results are plotted in log scale in (d). It should be noted that the data of compression (dash lines) creep-aging curves for T84 samples are too small to express in (c).

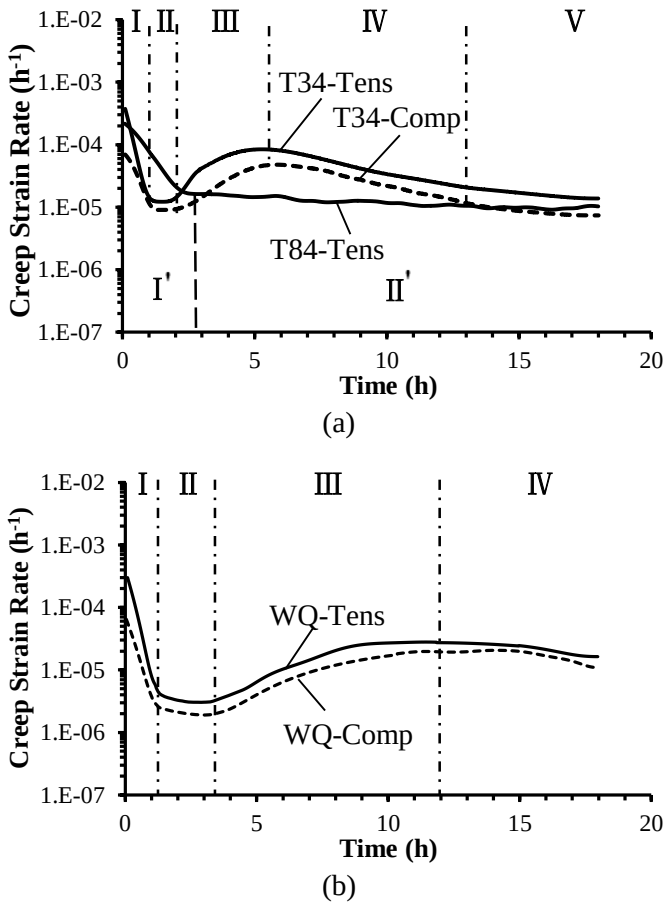

Figure 4. Tension (solid lines) and compression (dash lines) creep strain rate curves for initial tempers of (a) T34 and T84, and (b) WQ under 150 MPa in 18 h.

The tension and compression creep-ageing curves show a similar trend based on the creep strain rate evolution, but the magnitude of creep strains is different. A more significant initial primary creep stage (stage I) is observed in tension creep-ageing tests than that in compression ones for the T34 and WQ alloys. In fact, the initial primary creep strains are very low for T34 specimens under compressive loads and are difficult to recognise from creep strain curves. In the subsequent stages of the tests (after 3 hours), the creep strains tend to be 1.5 to 3 times larger in tension than that in compression for the T34 and WQ alloys. However, for the T84 initial condition, the amount of creep deformation is found insignificant under compressive stresses of 150 and 175 MPa. To show more details of the compressive creep curves in Fig. 3(c), their creep strains are plotted in log scale in Fig. 3(d). It can be discerned that the compressive creep strain is less than 0.002% after 18 h creep-ageing. In addition, Fig. 3 also shows that with the higher stress level (175 MPa), larger creep strains were generated during the tests for AA2050 with all three initial tempers (T34, WQ and T84).

3.2 Age hardening phenomena

The hardness test results for pure ageing of the as-received alloy (T34) at 155 °C are shown in Fig. 5(a). The hardness curve during the ageing period illustrates a reversion phenomenon at the early stage and an obvious age-hardening at the later stage. The peak strength appears around 18-19 h of the ageing time, which corresponds well to the data from the material supplier.

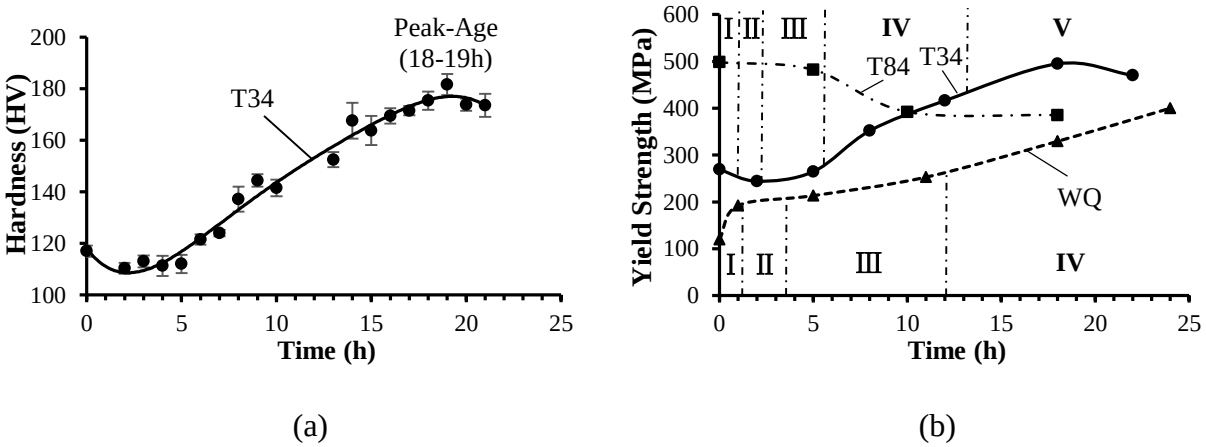

(a) (b)

Figure 5. (a) Hardness curve for pure ageing (error bars display the standard deviation from 5 repeating measurements) and (b) yield strength curves against creep-ageing time for different initial tempers after 150 MPa tension creep-ageing tests.

The evolution of yield strengths for specimens with initial tempers of T34, WQ and T84 after creep-ageing tests is plotted in Fig. 5(b). The five and four creep stages for corresponding T34 and WQ initial temper conditions introduced in section 3.1 are also marked on the figure according to the creep-ageing time. In stage I and II, a decrease of yield strength occurs in T34 sample, while WQ sample experiences an increase of the yield strength without the reversion. Moreover, it can be observed that in the corresponding stage III for T34 and WQ samples, where an increasing creep strain rate is present, both yield strength curves demonstrate a comparatively stable period with only a minor increase. While in stage IV, the yield strengths increase significantly in both temper conditions until the peak strength is reached. For the T84 sample, its yield strength experiences a continuous decrease with increasing ageing time.

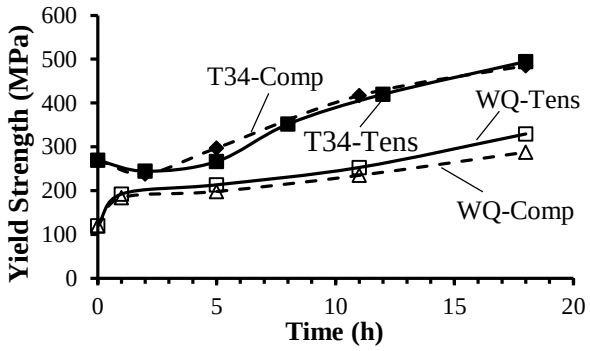

(a)

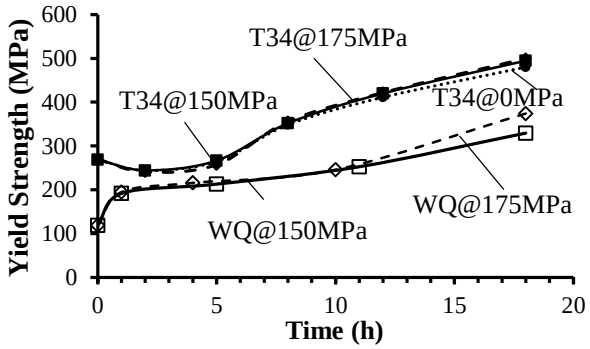

(b)

Figure 6. Effect of creep-ageing stress direction and stress level on the yield strength of T34 and WQ initial tempers. (a) Creep-aged under 150 MPa tension (solid line) and compression (dash line); (b) creep-aged under tensile stresses of 0 MPa (dot line), 150 MPa (solid line) and 175 MPa (dash line).

Fig. 6(a) shows the comparison of yield strengths after tension and compression creep-ageing tests. For the T34 alloy, the whole curves demonstrate similar variations during both tension and compression creep-ageing tests although the yield strengths show a slight difference at the creep-ageing time of 5 h. While for the WQ material, the yield strengths under compressive stresses are slight lower than those under tensile stresses for same ageing times. The effects of stress levels (0, 150 and 175 MPa) on the yield strength of AA2050 during tensile creep-ageing tests are plotted in Fig. 6(b). For T34 material, almost identical results of yield strength are observed under all creep-ageing stress levels (0, 150 and 175 MPa), while the yield strength of the WQ material is higher under 175 MPa than that under 150 MPa after 18 h tension creep-ageing. These results indicate that the stress directions and stress levels have little effects on mechanical properties of the creep-aged material with T34 initial temper.

3.3 Microstructure of selected creep-aged specimens

Fig. 7 shows the microstructures of the selected specimens with T34 initial temper before and after creep-ageing tests. The as-received material has a significant amount of dislocations caused by the pre-stretch (Fig. 7 (a)), but no apparent precipitates were observed. After 5 h tensile creep-ageing under 150 MPa, thin platelets of T_1 phase and θ' phase are observed (Fig. 7 (b)). The microstructural characterisations for T_1 phase and θ' phase are illustrated in Supplementary Figs. 2 and 3, respectively. The S phase can be occasionally observed as illustrated in Supplementary Fig. 4. After 18 h tensile creep-ageing under 150 MPa, copious T_1 and θ' precipitates appear as shown in Fig. 7(c). The significant growth, both at length and thickness directions, of T_1 precipitates from 5 h to 18 h creep-ageing can also be identified from the bottom-right inserts in Figs. 7(b) and (c). Fig. 7(d) shows the precipitate distribution of the compressive creep-aged specimen for 18 h under 150 MPa, which is overall similar to that in Fig. 7(c) (mainly T_1 and θ' phases, with minor S phase as well).

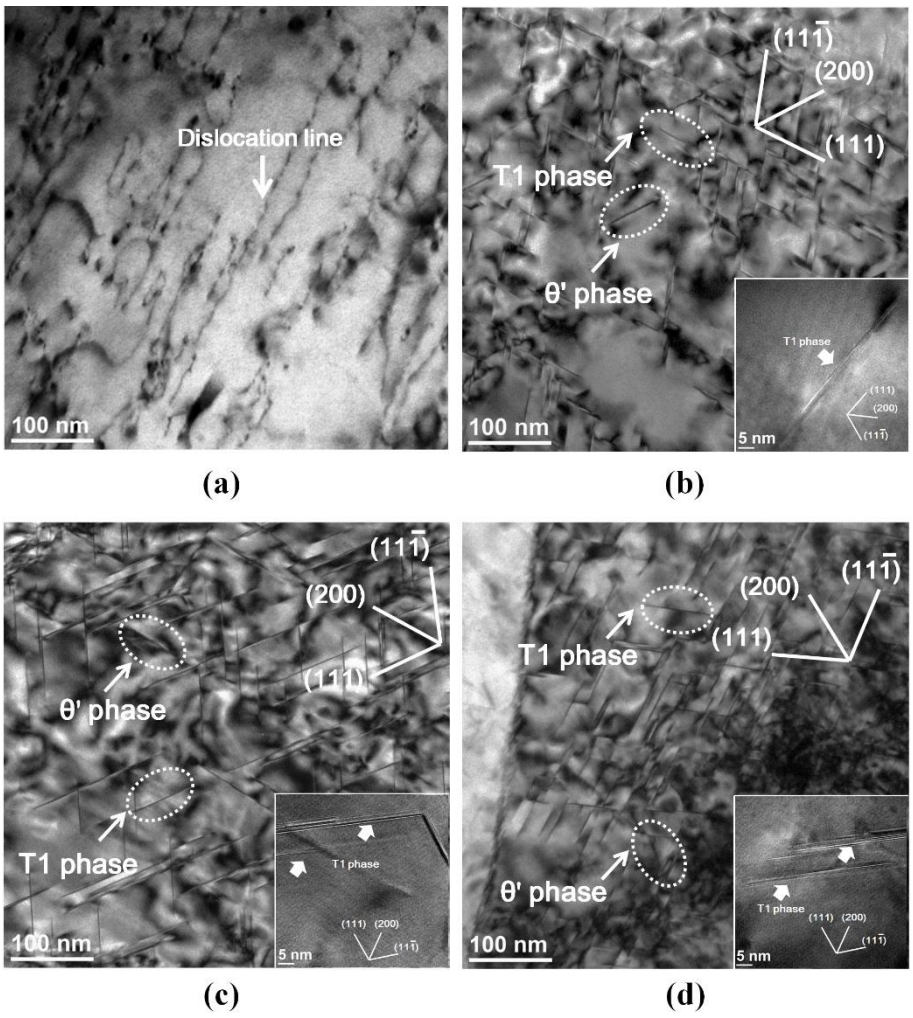

Figure 7. TEM images of the selected specimens: (a) as-received, (b) 150 MPa tension creep-aged for 5 h and (c) 18 h, and (d) 150 MPa compression creep-aged for 18 h. The bottom-right images in (b), (c) and (d) showing the features of T_1 precipitates.

In addition, the θ’ phases were found to preferentially nucleate at a particular variant under [100] zone axis of fcc matrix in both the tensile and compressive creep-aged samples, as shown in Fig. 8. Particularly, the habit plane of θ’ phase demonstrates a small angle with the tensile stress direction (Fig. 8 (a)), while under the compressive stress conditions, the habit plane of θ’ phase has a much larger angle with the load direction, tending to be more perpendicular to the compression direction, as shown in Fig. 8 (b).

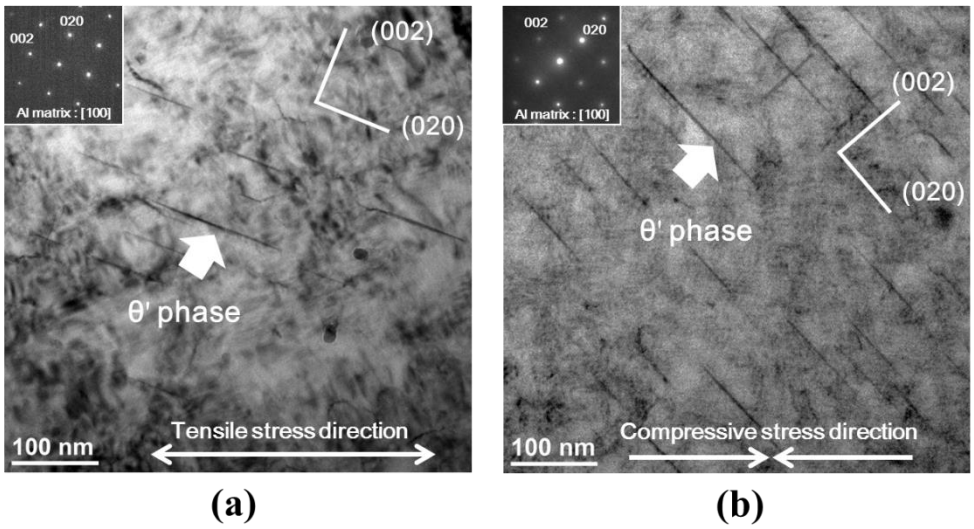

Figure 8. TEM images of the oriented θ’ phase in [100] zone axis of fcc matrix in (a) tensile and (b) compressive creep-aged samples under 150 MPa for 18 h.

4. Discussion

4.1 Tensile creep-ageing behaviour with T34 initial temper

It is known that most alloys can fit into two categories according to their creep behaviour: class I alloys (no primary or inverse primary creep behaviour) and class II alloys (normal primary creep behaviour) [22, 23]. Generally, both categories demonstrate the conventional creep behaviour throughout the whole creep life, including the primary stage, steady-secondary stage and tertiary stage [22]. The experiments carried out in this work, like other CAF works, are within the first two creep stages.

As shown in Figs. 3(a) and 4(a), the special five-stage creep-ageing behaviour of T34 sample, which was observed in aluminium alloys for the first time in this study, can be described as the “double primary creep feature”. More specifically, a conventional creep behaviour including an initial primary creep stage (stage I) and a transient steady creep stage (stage II) occurs in the first 2 h of creep-ageing tests. Subsequently an intermediate inverse creep stage (stage III) with an increasing creep strain rate follows. After that, the creep strain rate tends to decrease again until it reaches a relatively stable level, which is termed as the

second primary creep stage (stage IV) and the followed second steady creep stage (stage V), as schematically presented in Fig. 9. Unlike the conventional two-stage creep-ageing behaviour, this new "double primary creep feature" of AA2050 cannot be explained by the dislocation mechanism alone, the diffusion mechanism, including precipitates and solid solutes evolution, apparently plays a vital role.

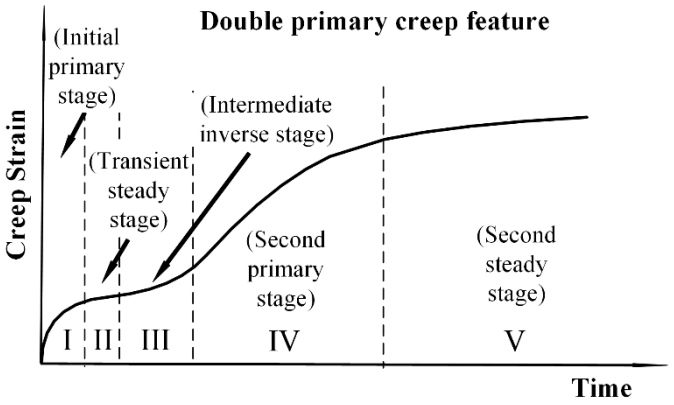

Figure 9. Schematic of "double primary creep feature" for AA2050 with T34 initial temper.

From the microstructural results of the selected creep-aged specimens in section 3.3 and some other literatures which show similar results [8, 24, 25], the evolution of precipitates and material strength during the whole ageing process of AA2050 with T34 initial temper can be divided into several regions, as shown schematically in Fig. 10. These regions include: (i) a dissolution region ($t_0 - t_1$) where the existing precipitates formed during natural ageing in the T34 temper, are dissolved at the beginning of artificial ageing (although no apparent precipitates were observed in Fig. 7(a) in this study due to the resolution limit of the current TEM, the small Cu clusters proposed by an earlier study [24] with a similar material should exist after natural ageing); (ii) a nucleation period ($t_1 - t_2$) of T_1 precipitates whose nucleation is significantly accelerated by the dislocations, which are induced by the pre-stretch; (iii) a growth period ($t_2 - t_4$) of T_1 and θ' precipitates when they coexist and compete with S precipitates until rising to dominance at the peak-aged state; and (iv) a coarsening period of T_1 precipitates (after t_4) where over-ageing occurs. The corresponding microstructural evolution is depicted schematically in Fig. 10(b). The detailed features of the precipitates at the times of t_0, t_2, and t_4 correspond well with the TEM results of 0, 5 and 18 h tensile creep-aged specimens in Fig. 7 respectively.

The yield strength curves as well as their corresponding precipitate evolution stages are illustrated in Fig. 10(a). Compared with Fig. 5(b), it can be noticed that the nucleation period

of T_1 precipitates coincides with the creep stage III where creep strain rate increases, indicating a relationship between them.

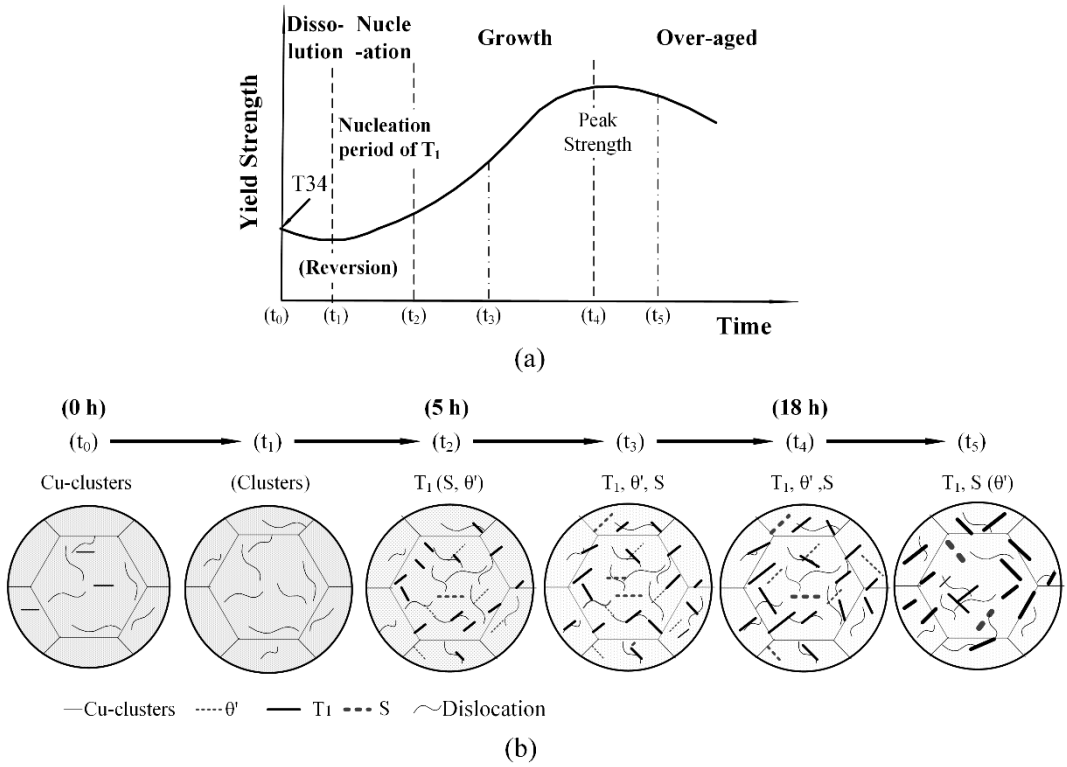

Figure 10. Evolution of (a) yield strength and (b) microstructure during creep-ageing tests with T34 initial temper, with corresponding ageing steps.

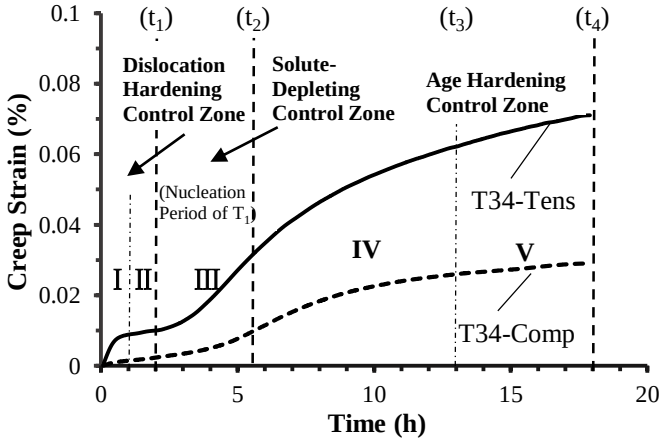

Figure 11. Tension and compression creep-ageing curves (T34 initial temper, 150 MPa) with corresponding ageing steps.

Creep deformation is generally induced by the dislocation motion and the diffusion mechanism which are mainly controlled by dislocations, solute-matrix bonding and precipitates [26, 27]. In order to assist further analysis, the creep strain curves are superimposed onto the related ageing steps, which are associated with the testing time, as

shown in Fig. 11. As illustrated in Fig. 11, though the dissolution of precipitates appears in the first 2 h of creep-ageing tests, the dislocation hardening, which is generated to a saturation level by creep deformation, still plays a dominant role in determining the creep behaviour during this period, leading to the initial normal primary creep stage (stage I) with a fast decreasing creep strain rate and the transient steady creep stage (stage II). During the intermediate inverse creep stage (stage III), solutes are fast depleted because of the accelerated nucleation of T_1 precipitates on high energy sites offered by the existing dislocations, contributing to a decrease of the creep resistance of the material [23, 28]. Consequently, it is possible to induce an increase of the creep strain rate in this stage, if the solute-depletion softening overrides the age hardening effect of the T_1 nuclei. However, more studies are needed in this area in order to fully understand the detailed mechanism.

As ageing goes on, the growth of T_1 precipitates begins to control the hardening progress of the alloy, the age hardening mechanism then determines the creep behaviour in the second primary creep stage (stage IV). The growth of T_1 precipitates offers stronger resistance to the movement of dislocations and decreases the creep strain rate until it reaches a stable level in the second steady creep stage (stage V). Thus the dislocation and diffusion mechanisms together determine the new "double primary creep feature" of AA2050 with T34 initial temper during creep-ageing tests.

4.2 Effect of stress direction on creep-ageing behaviour

Fig. 3 has demonstrated that creep strains in tension conditions are larger than those in compression during creep-ageing tests of AA2050, although their evolution trends are similar. This is true for tests with all initial tempers. It is known that both the creep and ageing behaviour during CAF process are mainly determined by the evolution of precipitates and dislocations, while precipitate properties, such as their orientations, are affected by the direction of applied stresses [15, 29]. Therefore, the different precipitates behaviour determined by stress directions should play an important role in the asymmetric tension and compression creep-ageing behaviour.

It has been shown in earlier studies [15, 29, 30] that the negative precipitate-matrix misfits of θ' precipitates can lead to the oriented-phenomena of the precipitates in stress-ageing conditions. The orientation has the tendency to be parallel with the tensile stress direction. While under compressive creep-ageing conditions, the orientation tends to be perpendicular to the load direction. The tendency of the preferred nucleation orientations of the θ' phases has also been observed in both tensile and compressive creep-ageing tests in this study (Fig.

8), which can be explained by the negative misfits as well. It has been reported that the dislocation motion, which leads to the creep deformation during creep-ageing tests, is strongly impeded by the interfaces of precipitates perpendicular to the load direction [27]. As the θ' precipitates play an important role in the creep-ageing process of the material, and more interfaces of θ' precipitates perpendicular to the stress direction can be obtained in compression creep-ageing conditions, where much larger angles between the precipitates and the load direction can be formed(Fig. 8(b)) than that in tensile stress conditions, a larger creep resistance is obtained in compression creep-ageing. Moreover, unlike tensile stresses, with compressive stresses in the material, the negative precipitate-matrix misfits of the main precipitates (including θ' and T_1) along the stress direction will also be increased, thus increasing the stress field around the precipitates and further reducing creep by hindering the shear or bypass of dislocations around it. These factors will lead to an increase of the creep resistance when compressive stresses are applied, which is also known as increasing the threshold stress of creep [31]. Consequently, lower creep strains will be present in compression creep-ageing tests, as shown in Fig. 3.

The negligible creep strain in compression creep-ageing tests of the T84 alloy (Fig. 3(d)) is possibly due to the increased threshold stress for creep. Significant strengthening of the fully developed precipitates has already taken place in this temper before creep-ageing. As discussed earlier, with the compressive stress, a larger threshold stress for creep is introduced, which may be comparable with the applied stresses in this study, resulting in little creep deformation.

4.3 Effect of stress level on creep-ageing behaviour

The strengthening phenomenon of the alloy during CAF process is mainly caused by the precipitation and dislocation hardening [26]. It was reported that higher stress levels in creep-ageing tests can not only accelerate the ageing progress, but also enhance the dislocation hardening effects by introducing larger creep strains [26]. The similar phenomena were observed for the WQ alloys, where larger applied stresses generate higher creep deformation at the same testing time (Fig. 3(b)) and lead to larger yield strengths at a longer ageing time (Fig. 6(b)).

Nevertheless, for the T34 alloy investigated in this study, it is found that the strengthening progresses are very similar under both stress-free and stress-applied conditions, which indicates that the stress induced dislocation hardening plays a minor role in the strength evolution (Fig. 6(b)). Moreover, it has been shown that the pre-stretch, which is not done for

the WQ alloys, controls the ageing progress of Al-Cu-Li alloys largely, increasing the maximum yield strength and shortening the ageing time [32, 33]. Furthermore, Cassada et al. [33] have investigated the effects of different pre-stretch levels and observed that there is a limit of the pre-stretch level, above which the age hardening progress would be hardly affected by further increasing pre-stretch levels, specifically, for the Al-2.45Cu-2.45Li alloy, the limit is about 6%. For the AA2050 in this study, the 3.5-4.5% pre-stretch in the T34 initial temper may have reached the limit level and thus stress levels can hardly change the precipitation hardening progress during creep-ageing tests. Therefore, although more dislocations will be generated with increasing applied stress levels, little differences in the strengthening progress would be observed for the T34 material. Meanwhile, the creep deformation will be increased with more dislocations generated, as shown in Fig. 3.

4.4 Effect of initial temper on creep-ageing behaviour

The creep-ageing behaviour of the material was largely affected by its initial temper condition. Different creep strain and yield strength variations were observed in the materials with T34, WQ and T84 initial tempers, as shown in Fig. 3 and Fig. 5(b).

The creep-ageing behaviour of the WQ material presents an extended "double primary creep feature", which is similar to T34 material, as shown in Figs. 3(a) and 3(b). The precipitates appearing during the creep-ageing of both WQ and T34 materials should be similar, mainly including Cu clusters, θ', S and T_1 [11, 32, 33]. However, the evolution progress of those precipitates will show differences because of the lacking of natural-ageing and pre-stretch in the WQ material. Without natural-ageing in the WQ material, new precipitates will nucleate when artificial-ageing begins, resulting in a strengthening phenomenon, rather than initial softening in the T34 material, as shown in Fig. 5(b). Consequently, combining this strengthening behaviour with the dislocation hardening effects at the initial stage of creep-ageing tests, more apparent primary creep stages can be observed in both tension and compression creep-ageing tests with the WQ material than that with the T34 material, as demonstrated in Figs. 3(a) and 3(b). Moreover, without initial dislocations caused by the pre-stretch in the WQ material, directly nucleation of T_1 and θ' phases becomes much harder than that in T34 material, resulting in a much longer nucleation and growth time for those precipitates [24], leading to the extended "double primary creep feature" in the WQ material. The diffusion related solute-depleted softening mechanism may still play its role in the creep-rate controlling during this period but in a more gentle way, leading to the longer intermediate inverse creep stage (stage III in Fig. 3(b)) with a gradual increase of the creep

strain rate. Afterwards, the creep strain rate starts to decrease in the second primary creep stage (stage IV in Fig. 3(b)) as age hardening by the growth of T_1 and θ' precipitates become more and more significant. A second steady creep stage (stage V) should follow because of the continuing but gradually less increasing age hardening effects. However, this stage was not observed within the test period of up to 18 h in this study.

However, the creep-ageing behaviour of the T84 alloy is different from those of T34 and WQ ones. Its hardening behaviour is shown in Fig. 5(b) and can be referenced from t_4 to t_5 in Fig. 10(a). During creep-ageing tests in this condition, coarsening of T_1 precipitates is the dominant microstructural change. As little solutes will diffuse from the matrix after peak ageing, dislocations and precipitates become the main factors affecting the creep-ageing behaviour. Its creep-ageing curve then demonstrates the typical two-stage creep-ageing behaviour: a primary creep stage (stage I') controlled by the dislocation hardening and a steady secondary creep stage (stage II') caused by the balance between the dislocation hardening and the recovery [26], as shown in Fig. 3(c).

5. Conclusions

Creep-ageing behaviour of AA2050 has been experimentally studied under both tension and compression conditions with three initial temper conditions (T34, T84 and WQ) and the microstructure of selected specimens have been examined using TEM. The following conclusions can be drawn:

(1) A new "double primary creep feature" consisting of five creep stages is observed for AA2050 with T34 initial temper. The initial primary and transient steady creep stages are controlled by the dislocation hardening, the intermediate inverse creep stage with an increasing creep strain rate is controlled by the diffusion related solute-depleting mechanism, and the second primary and second steady-state creep stages are controlled by the subsequent age hardening.

(2) Tension creep-ageing generates a significant higher initial primary creep and about 1.5 to 3 times larger creep strains in subsequent creep stages compared with the compression creep-ageing at the same stress level for AA2050 with T34 and WQ initial tempers. The trend of the curves, however, is similar under both stress directions.

(3) Higher stress level increases the creep strain of AA2050 with all initial tempers. Both stress levels and stress directions affect age hardening progress of AA2050 with WQ initial temper, while contribute little change to the strength of the alloy with T34 initial temper.

(4) The WQ material shows a similar creep-ageing behaviour to that of the T34, but with longer period for each creep stages, due to lacking of initial pre-stretch/natural ageing after quenching. It does not reach peak strength within 18 h under the conditions studied.

(5) The peak-aged T84 temper exhibits the typical two-stage creep-ageing behaviour under tensile stresses, while little creep strain (less than 0.002%) was observed after 18 h compression creep-ageing.

Acknowledgements

The authors would like to thank the financial support from ESI Group (France). The material was provided by Embraer (Brazil) and the specimens were machined through ESI Group. Their contributions are greatly appreciated. Mr Y. Li would also like to thank the support from the Chinese Scholarship Council (CSC).

References:

[1] L.H. Zhan, J.G. Lin, T.A. Dean, M.H. Huang, Int J Mech Sci, 53 (2011) 595-605.
[2] R. Arabi Jeshvaghani, M. Emami, H.R. Shahverdi, S.M.M. Hadavi, Materials Science and Engineering: A, 528 (2011) 8795-8799.
[3] R.A. Hafley, (No. NASA/TM-2011-217163) National Aeronautics and Space Administration, Langley Research Center, 2011.
[4] P. Lequeu, K.P. Smith, A. Daniélou, J. Mater. Eng. Perform., 19 (2010) 841-847.
[5] R. Yoshimura, T.J. Konno, E. Abe, K. Hiraga, Acta Mater., 51 (2003) 2891-2903.
[6] R. Yoshimura, T.J. Konno, E. Abe, K. Hiraga, Acta Mater., 51 (2003) 4251-4266.
[7] S. Wang, M. Starink, Int. Mater. Rev., 50 (2005) 193-215.
[8] K.S. Kumar, S.A. Brown, J.R. Pickens, Acta Mater., 44 (1996) 1899-1915.
[9] F.W. Gayle, F.H. Heubaum, J.R. Pickens, Scr. Metall. Mater., 24 (1990) 79-84.
[10] K.S. Kumar, S.A. Brown, J.R. Pickens, Scr. Metall. Mater., 24 (1990) 1245-1250.
[11] B.M. Gable, A.W. Zhu, A.A. Csontos, E.A. Starke Jr, J. Light Met., 1 (2001) 1-14.
[12] S.M. Kazanjian, N. Wang, E.A. Starke Jr, Mater. Sci. Eng., A, 234–236 (1997) 571-574.
[13] K.C. Ho, J. Lin, T.A. Dean, International Journal of Plasticity, 20 (2004) 733-751.
[14] C. Li, M. Wan, X.-D. Wu, L. Huang, Materials Science and Engineering: A, 527 (2010) 3623-3629.
[15] T. Eto, A. Sato, T. Mori, Acta Metall., 26 (1978) 499-508.
[16] B. Skrotzki, G.J. Shiflet, E.A. Starke, Jr., Metall. Mater. Trans. A, 27 (1996) 3431-3444.
[17] A.W. Zhu, J. Chen, E.A. Starke Jr, Acta Mater., 48 (2000) 2239-2246.
[18] A.W. Zhu, E.A. Starke Jr, Journal of Materials Processing Technology, 117 (2001) 354-358.
[19] G.J. Heimerl, J. Farquhar, (No. NASA-TN-D-160) National Aeronautics and Space Administration, Langley Research Center, Langley Field, VA., 1959.
[20] Q. Zhang, W. Zhang, Y. Liu, Mater. Sci. Eng., A, 628 (2015) 340-349.
[21] J. Przydatek, Imperial College London (PhD thesis), 1998.
[22] F.A. Mohamed, T.G. Langdon, Acta Metall., 22 (1974) 779-788.
[23] O.D. Sherby, P.M. Burke, Prog. Mater. Sci., 13 (1968) 323-390.
[24] B. Decreus, A. Deschamps, F. De Geuser, P. Donnadieu, C. Sigli, M. Weyland, Acta Mater., 61 (2013) 2207-2218.
[25] Z. Chen, K. Zhao, L. Fan, Mater. Sci. Eng., A, 588 (2013) 59-64.

[26] L. Zhan, J. Lin, T.A. Dean, M. Huang, Int. J. Mech. Sci., 53 (2011) 595-605.
[27] M.E. Kassner, M.-T. Pérez-Prado, Chapter 8 - Creep Behavior of Particle-Strengthened Alloys, in: M.E.K.-T. Pérez-Prado (Ed.) Fundamentals of Creep in Metals and Alloys, Elsevier Science Ltd, Oxford, 2004, pp. 151-169.
[28] O.D. Sherby, E.M. Taleff, Mater. Sci. Eng., A, 322 (2002) 89-99.
[29] A.W. Zhu, E.A. Starke Jr, Acta Mater., 49 (2001) 2285-2295.
[30] H. Hargarter, M.T. Lyttle, E.A. Starke, Mater. Sci. Eng., A, 257 (1998) 87-99.
[31] E.A. Marquis, D.C. Dunand, Scr. Mater., 47 (2002) 503-508.
[32] S.P. Ringer, B.C. Muddle, I.J. Polmear, Metall. Mater. Trans. A, 26 (1995) 1659-1671.
[33] W.A. Cassada, G.J. Shiflet, E.A. Starke, Metall. Trans. A, 22 (1991) 299-306.

Supplementary Material

A notched line (with the elongated cavity) was made by a knife to be parallel to the stress direction of CAF treatment in the TEM specimen as showm in Supplementary Fig. 1. The notched line in the TEM specimen was aligned to be perpendicular to the central line of TEM holder before inserting into TEM. The procedure can ensure the stress direction parallel to the horizontal direction of the TEM image.

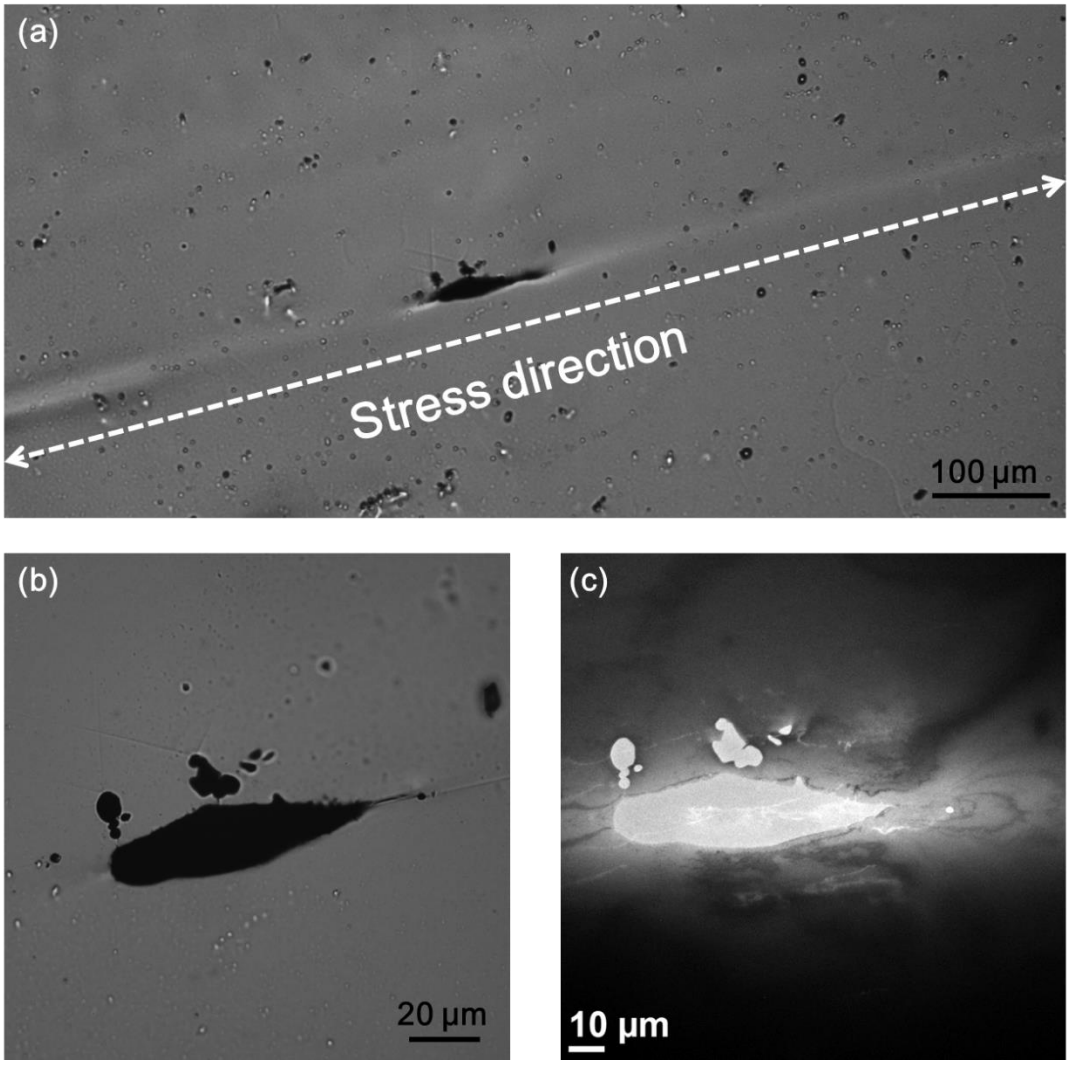

Supplementary Figure 1. (a) A low-magnification optical micrograph showing the notched line (parallel to the stress direction) and an elongated cavity, (b) an optical micrograph of the cavity, (c) a TEM micrograph of the cavity.

High-resolution TEM image of T1 phase was aligned in edge-on configuration of its habit plane (0 0 0 1) under the observation along the zone axis [1 $\bar{1}$ 0] of aluminium matrix as shown in Supplementary Fig. 2(a). From the fast Fourier transformed (FFT) diffractogram and the corresponding illustration as presented in Supplementary Fig. 2(b-d), the crystallography of T1 phase is determined as P6/mmm in hexagonal structure that is consistent with the model proposed by Huang and Ardell et. al [1]. The orientation relationship between T1 and aluminium matrix can be described as $(0001)_{T1}//(111)_{Al}$, $[1\bar{1}00]_{T1}//[1\bar{1}0]_{Al}$ [2]. Morphology of T1 phase is plate-like and prefers to grow along the {111} lattice plane of aluminium matrix.

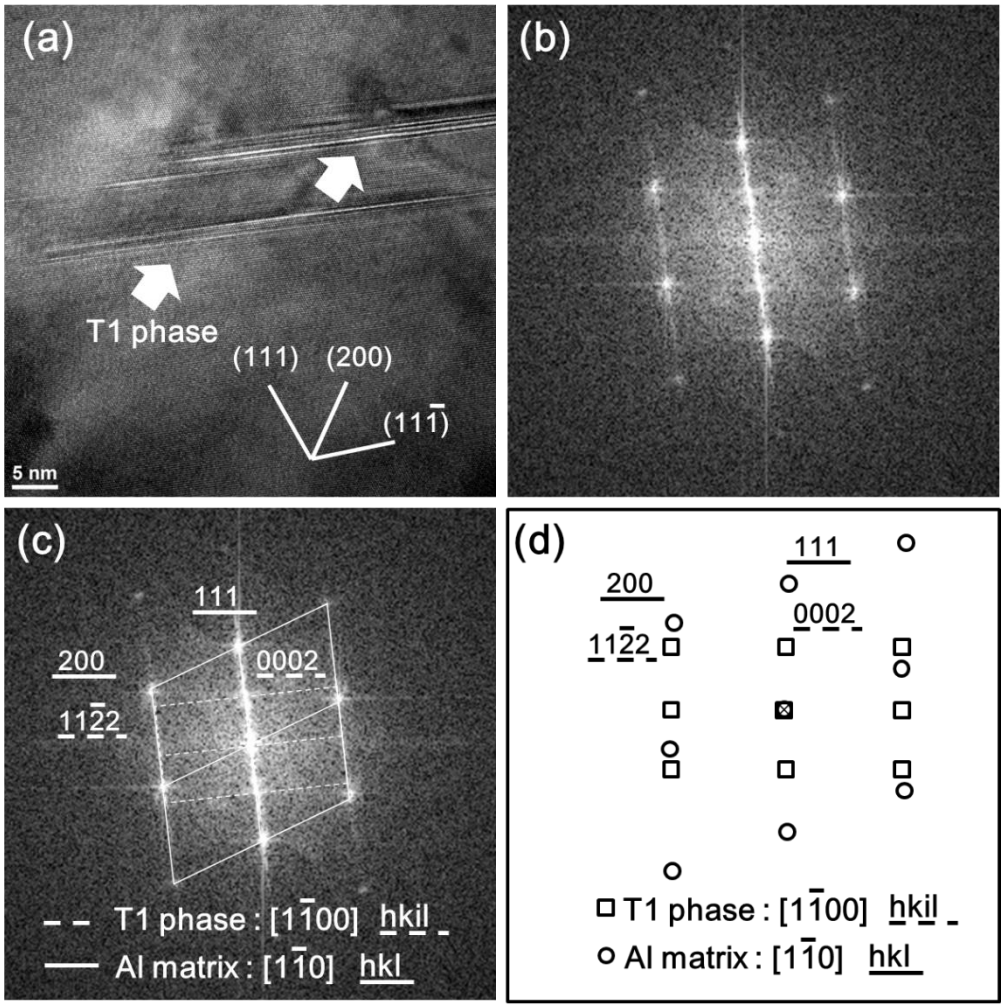

Supplementary Figure 2. (a) HR TEM image showing the T1 phase in Al matrix, (b) the corresponding FFT diffractogram for the T1 phase, (c) the orientation relationship between T1 phase and matrix, (d) the illustration for the identified spots of T1 phase and matrix in (b).

High-resolution TEM image of θ' phase was aligned in edge-on configuration of its habit plane (0 0 1) under the observation along the zone axis [0 1 0] of aluminium matrix as shown

in Supplementary Fig. 3(a). From the fast Fourier transformed (FFT) diffractogram and the corresponding illustration as presented in Supplementary Fig. 3(b-d), the crystallography of θ' phase is determined as $I\bar{4}m2$ in tetragonal structure that is consisten with the model proposed by B.C. Muddle et. al [3]. The orientation relationship between θ' and matrix is $(100)_{\theta'}//(100)_{Al}$, $[001]_{\theta'}//[001]_{Al}$ [2]. The morphology of θ' phase is also plate-like and prefer to grow along the {100} lattice planes of matrix.

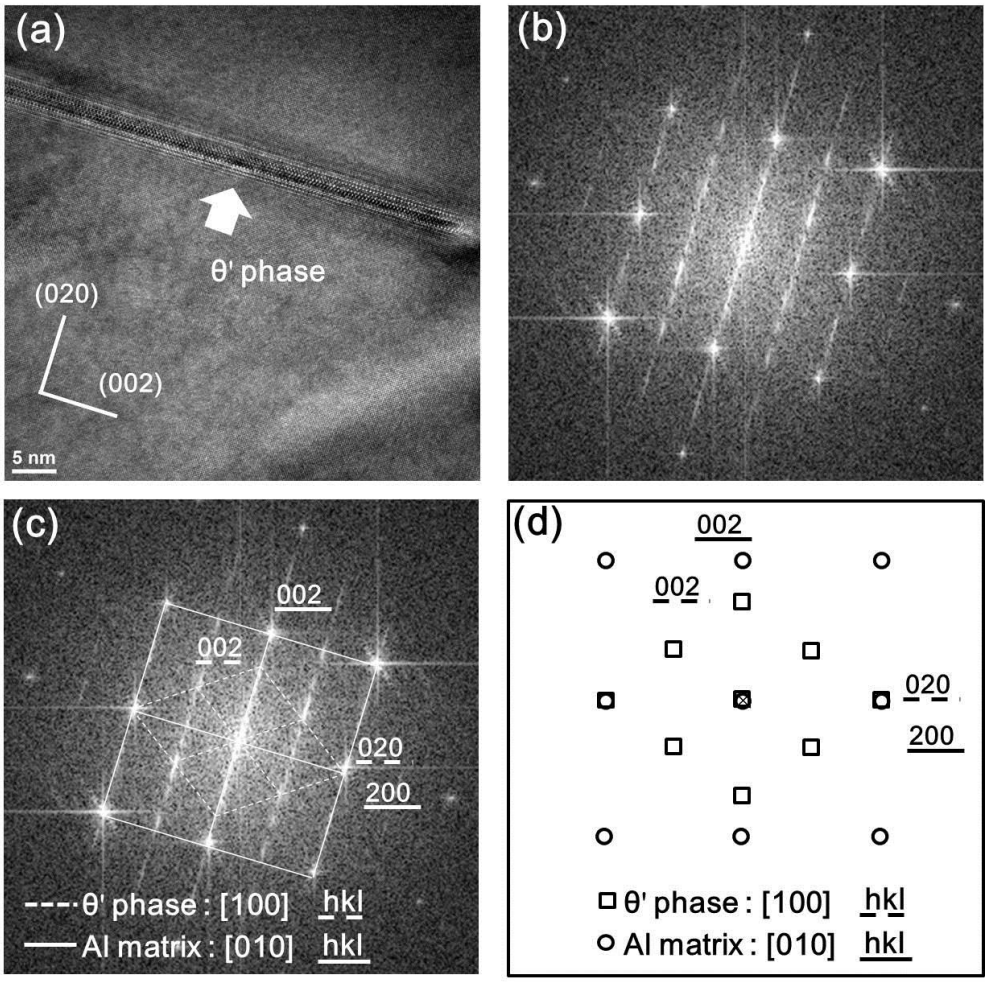

Supplementary Figure 3. (a) HR TEM image showing the θ' phase in Al matrix, (b) the corresponding FFT diffractogram for the θ' phase, (c) the orientation relationship between θ' phase and matrix, (d) the illustration for the identified spots of θ' phase and matrix in (d)

High-resolution TEM image of S phase under under the observation along the zone axis [100] of aluminium matrix as shown in Supplementary Fig. 4(a). From the fast Fourier transformed (FFT) diffractogram and the corresponding illustration for S phase as shown in Supplementary Fig. 4(b-d), the crystallography of S phase is determined as Cmcm in

orthorhombic structure that is consistent with Pearson's handbook [4], and the orientation relationship between S and matrix is $(010)_S//(02\bar{1})_{Al}$, $[100]_S//[100]_{Al}$ [2]. The morphology of S phase is also plate-like and grow along the {0 2 1} lattice planes of matrix.

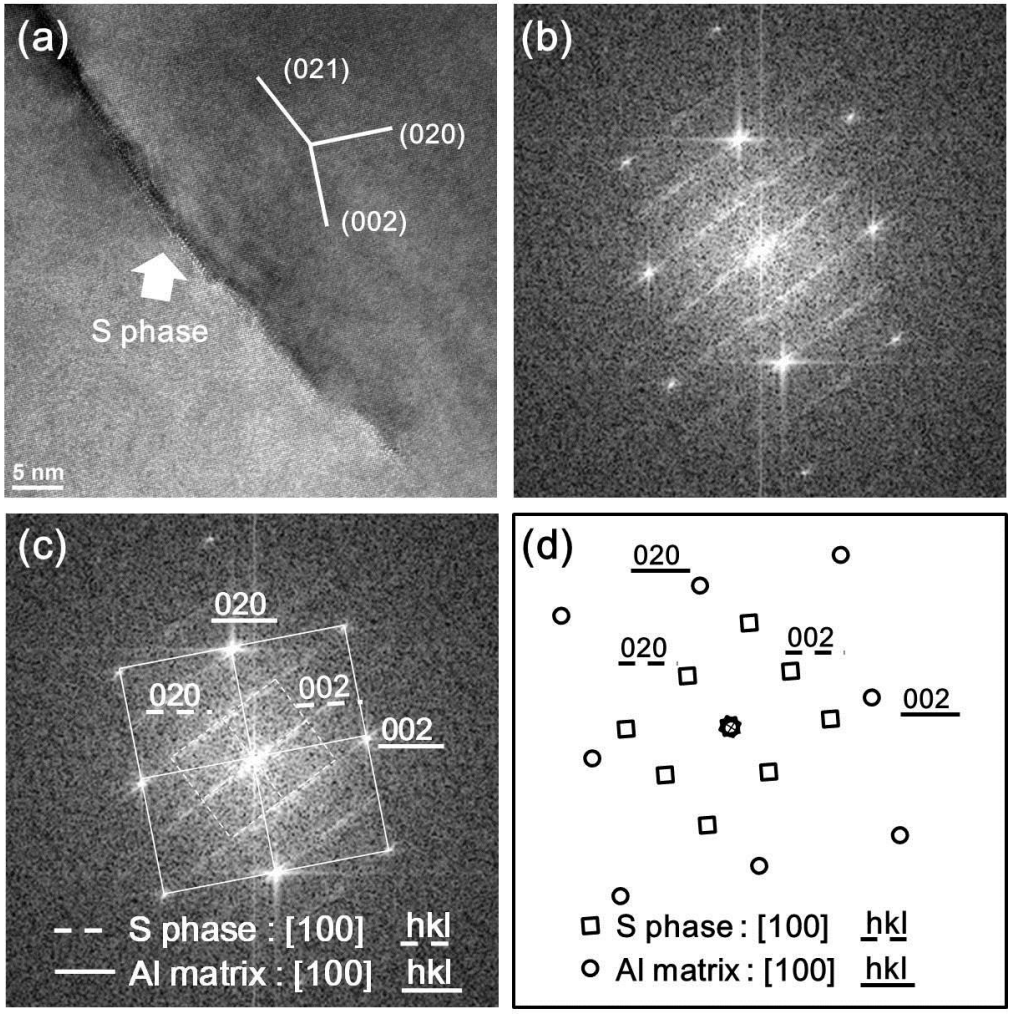

Supplementary Figure 4. (a) HR TEM image shows the S phase in Al matrix, (b) the corresponding FFT diffractogram for the S phase, (c) the orientation relationship between S phase and matrix, (d) the illustration for the identified spots of S phase and matrix in (c)

Reference:

[1] B.C. Muddle and I.J. Polmear, *Acta Metall. Mater.*, 37 (1989) pp.777-789.

[2] S.C. Wang and M.J. Starink, *Int. Mater. Rev.*, 50 (2005) pp.193-215.

[3] J.C. Huang and A.J. Aedell, *Mater. Sci. Technol.*, 3 (1987) pp.17-188.

[4] 'Pearson's handbook of crystallographic data for intermetallic phases', 2nd edn, (ed. P. Villars); 1991, Materials Park, OH, ASM International.